Sciencexpress Report

An All-Silicon Passive Optical Diode

Li Fan,[1,2]* Jian Wang,[1,2]* Leo T. Varghese,[1,2]* Hao Shen,[1,2] Ben Niu,[1,2] Yi Xuan,[1,2] Andrew M. Weiner,[1,2] Minghao Qi[1,2,3]†

[1]Birck Nanotechnology Center, Purdue University, West Lafayette, IN 47907, USA. [2]School of Electrical and Computer Engineering, Purdue University, West Lafayette, IN 47907, USA. [3]Shanghai Institute of Microsystem and Information Technology, Chinese Academy of Sciences, Shanghai 20050, China.

*These authors contributed equally to this work.

†To whom correspondence should be addressed. E-mail: mqi@purdue.edu

A passive optical diode effect would be useful for on-chip optical information processing, but has been difficult to achieve. Based on optical nonlinearity, we demonstrate a forward-backward transmission ratio up to 28 dB within telecommunication wavelengths using two 5-micrometer radius silicon rings. Our device is passive, yet maintains optical nonreciprocity for a broad range of input power levels and performs equally well even if the backward input power is higher than the forward input. The silicon optical diode is ultra compact and is compatible with current complementary metal-oxide-semiconductor (CMOS) processing.

Nonreciprocal transmission is fundamental in information processing. Electrical nonreciprocity, or diode effect, had been realized in integrated form with a semiconductor *p-n* junction. Optical nonreciprocity (ONR) is inherently difficult due to the time-reversal symmetry of light-matter interaction (*1*). Previously reported ONR has been based on magneto-optic effect (*2–4*), optical nonlinearity (*5–8*), electro-absorption modulation (*9*), cholesteric liquid crystals (*10*), optomechanical cavities (*11*), indirect interband photonic transitions (*12*) and opto-acoustic effect (*13*). CMOS compatible passive optical diodes with footprint and functionality analogous to *p-n* junctions, however, have not been realized at near infrared, the wavelength choice for silicon photonics. Our optical diode (Fig. 1A) is based on strong optical nonlinearity in high-quality-factor (*Q*) Si microrings (*14–17*). It consists of a high-*Q* all-pass notch filter (NF) operating near the critical coupling regime (*17*) (Fig. 1B) and an add-drop filter (ADF) (*14*, *16*, *18*) with asymmetric power coupling to the bus waveguides (Fig. 1C). The resonant wavelength of the NF is thermally tuned to match that of the ADF through the thermo-optic effect of silicon (*19*).

A microring accumulates optical energy at its resonant wavelength. Schematics in Fig. 1E and Fig. 1F show that light couples into the microring in the ADF through two different gaps, G_2 and G_3, respectively. With forward and backward input power being $P_{c,f}$ and $P_{in,b}$, respectively, the optical energy stored in the microring near its resonant wavelength, λ_{ADF}, are

$$U_{\text{forward}}(\lambda) = \frac{P_{c,f}}{Q_{G_2}} Q_{ADF}^2 K(\lambda) \quad (1)$$

and

$$U_{\text{backward}}(\lambda) = \frac{P_{in,b}}{Q_{G_3}} Q_{ADF}^2 K(\lambda) \quad (2)$$

where Q_{ADF} is the ring's loaded quality factor, Q_{G_2} and Q_{G_3} are power coupling quality factors which are exponentially proportional to the gap sizes, and $K(\lambda)$ is independent of propagation direction for a linear system (*14*).

The energy enhancement factor in the ring depends on the propagation direction due to our asymmetric design (Q_{G_2} ~ 300,000, Q_{G_3} ~ 192,000, and Q_{ADF} ~ 43,800, all through curve-fitting), and $(U_{\text{forward}}/U_{\text{backward}}) = (Q_{G_3}/Q_{G_2}) = 0.64$ for $P_{c,f} = P_{in,b}$. With high input power at $\lambda_0 = \lambda_{ADF}$, the power density inside the ring will be amplified substantially, due to its high *Q* factors and small radius, to induce optical nonlinearity in silicon (*20–23*) and red-shift the ring's resonance ($\lambda'_{ADF} > \lambda_0$, Fig. 1F). The amount of resonance shift for forward propagation, due to the lower energy stored in the ring, is smaller than that for the backward direction. Defining wavelength detuning as $\delta_{ADF}(\lambda_0) = 2Q_{ADF}[(\lambda_0 - \lambda'_{ADF})/\lambda'_{ADF}]$, we have $|\delta_{ADF,forward}(\lambda_0)| < |\delta_{ADF,backward}(\lambda_0)|$. This leads to a higher forward transmission, $T_{ADF,forward}(\lambda_0)$, than the backward one, $T_{ADF,backward}(\lambda_0)$, since

$$T_{ADF,forward}(\lambda_0) = \frac{1}{\delta_{ADF,forward}^2(\lambda_0) + 1} F \quad (3)$$

and

$$T_{\mathrm{ADF,backward}}(\lambda_0)=\frac{1}{\delta^2_{\mathrm{ADF,backward}}(\lambda_0)+1}F \quad (4)$$

where $F=4Q^2_{\mathrm{ADF}}/Q_{G_2}Q_{G_3}$ is independent of propagation direction. Therefore an ADF with asymmetric power coupling can function as an ONR device for strong optical inputs, and we call it the ONR initiator.

For the NF, the power transmission near its resonance (λ_{NF}) is

$$T_{\mathrm{NF}}(\lambda_0)=\frac{\delta^2_{\mathrm{NF}}(\lambda_0)+\left(1-2Q_{\mathrm{NF}}/Q_{G_1}\right)^2}{\delta^2_{\mathrm{NF}}(\lambda_0)+1} \quad (5)$$

where Q_{NF} is the loaded quality factor of the NF ring and $\delta_{NF}(\lambda_0) = 2Q_{NF}[(\lambda_0 - \lambda_{NF})/\lambda_{NF}]$ is wavelength detuning. Our design leads to $Q_{G_1} \sim 55{,}000$ (*24*) and the fabricated NF ring (*25*) has $Q_{NF} \sim 27{,}000$, so $\left(1-2Q_{\mathrm{NF}}/Q_{G_1}\right)\approx 0$. A weak input will pass the NF with a strong attenuation of ~20 dB at $\lambda_0 = \lambda_{NF}$ since $\delta_{NF}(\lambda_0) = 0$. A strong input will red-shift the NF ring ($\lambda'_{NF} > \lambda_0$), resulting in a non-trivial $\delta'_{NF}(\lambda_0)$ and will pass the NF with a much smaller attenuation at λ_0 (Fig. 1D). We call the NF an ONR amplifier since it will significantly attenuate the weakened signal that has passed the ONR initiator in the backward direction.

When we cascade the ONR amplifier to an ONR initiator with similar onset power for nonlinearity (Fig. 1A), strong ONR can be achieved for a broad range of forward and backward input power levels. Without nonlinear effects, i.e. at a very low input power of ~85 nW at the device (1 μW measured at the input laser), our optical diode has a transmission that is independent of propagation direction (Fig. 1H).

With the input power increased to ~85 μW, a nonreciprocal transmission ratio (NTR) of ~20 dB was observed at $\lambda_0 = 1630$ nm (Fig. 1I). For forward propagation, input from port I enters the NF first, and has sufficiently high power to red-shift the NF resonance, thus allowing it to pass with low attenuation at wavelength λ_0 (solid curve in Fig. 1D). When it reaches the ADF, due to the large gap of G_2, as well as the power reduction after passing the NF, the optical energy accumulated in the ADF ring is not high enough to appreciably red-shift the resonance, i.e. $\delta_{ADF,forward}(\lambda_0) \rightarrow 0$ in Eq. 3. Thus light can transmit to the drop port through the resonance, and achieve reasonably high transmission in port II at λ_0 (solid curve in Fig. 1E). For backward propagation (input at port II), light will enter the ADF first. With the small gap, G_3, the energy in the ADF ring is high enough to red-shift its resonance, i.e. $|\delta_{ADF,backward}(\lambda_0)| > 0$ in Eq. 4, and transmitted light at λ_0 will be reduced (Fig. 1F, solid curve). At the NF, the reduced light intensity, due to both the resonance shift and the insertion loss of the ADF, will not be able to red-shift the NF ring, i.e. $\delta_{NF}(\lambda_0) \rightarrow 0$ in Eq. 5, and its intensity will be significantly reduced as it passes through the critically coupled NF at resonance ($\lambda_0 = \lambda_{NF}$, Fig. 1G).

At higher input power levels (~850 μW and ~2,100 μW), larger NTRs up to 29 dB was observed (Fig. 2). This is due simultaneously to the increase of the NTR from the ADF (compared to Fig. 1F which occurs at a rather moderate input power of ~85 μW) and to the sustained large NTR from the NF at high input power levels. Figure 3 shows the forward and backward transmissions of an individual ADF with coupling gaps of 420 nm and 630 nm (without a cascaded NF). In the forward direction, the transmitted power increases with the laser input power near resonance (~1550.4nm), while the backward transmitted power remains approximately the same, effectively increasing the NTR. In our optical diode (Fig. 1A), such saturation limits the backward input power entering the NF ($P_{c,b}$ in Fig. 1G). This restricts the nonlinearity in the NF and allows it to maintain high attenuation of the backward transmission.

The performance of our diode is independent of optical bistability (*7*, *20*, *26*), and is free from uncertainties caused by data acquisition schemes. In the spectra taken at two different scan modes of the tunable laser source (Fig. 2A), the solid lines are the spectra of a continuous-mode scan, which typically follows the upper trace of the hysteresis loop, while the dashed lines are the spectra of the stepped-mode scan, which is equivalent to a step-by-step changing of operating wavelength and generally follows the lower trace of the hysteresis loop. The rapid swing near 1630.1 nm indicates the transition between the upper and lower traces, possibly due to the fluctuations of laser power and wavelength in stepped-mode scan. Our optical diode does not operate in the bistability regime, and we observed almost identical NTRs with point measurements, i.e. fixing the laser at a specific wavelength and then measuring the transmitted power level at forward and backward directions (table S1).

The device operation is robust against the mismatch of resonant wavelengths between the two filters, and it can achieve strong ONR for various input power levels at a fixed wavelength. Within a resonance mismatch range of ~0.04 nm, the NTR remains over 25 dB (Fig. 4A). Given such tolerance, we were able to fix the operating wavelength of the diode by tuning the NF resonance in the backward direction to 1630.011 nm and achieve at least 18 dB of NTR for input power between 85 μW and 2,100 μW (Fig. 4B).

An electronic diode blocks the backward current for a large range of applied backward voltages. Analogously, table S1 shows that our optical diode attenuates the backward transmitted power to a low level (around –50 dBm) for a broad range of laser input power (5 dBm ~ 14 dBm) at the operating wavelength of 1630.011 nm. The forward

transmitted power is more than 20 dB higher than the backward transmitted power within this laser power range. Therefore our optical diode tolerates not only input power variation, but also forward/backward input power disparity.

Similar to all resonance-enhanced optical devices, our all-silicon optical diode is bandwidth limited. However its operating wavelength can be thermally tuned (*19*) and should work across a large wavelength band. It also has a relatively high insertion loss after subtracting the coupling losses (~10.7 dB per facet). For laser input power levels between 5 dBm and 10 dBm the forward insertion losses were ~12 dB. This number could be reduced if the intrinsic quality factor of both rings is increased to 250,000 (*16*, *17*), and if the thermal isolation of the rings is improved, such as by suspending the NF ring away from the substrate (*27*).

The optical nonlinear effects in silicon include Kerr effect (*28*, *29*), two-photon absorption (TPA) (*30*), free carrier effect (FCE) (*31*), and thermo-optic effect (*26*) from Joule heat generated through TPA, FCE and linear absorption. Due to the large thermal dissipation time of the SiO_2 under-cladding (~2 μs) (*21–23*), and the input power at tens of microwatts, the thermo-optic effect was dominant in our experiments. In addition to its role in enabling low power operation, the slow response time of the thermo-optic effect (which reacts to optical powers averaged over a μs range) may benefit one-way transmission of high-modulation-speed data streams, since the long integration time should desensitize nonlinear operation to fluctuations associated with rapidly varying data patterns or different modulation formats. Alternatively, when the slower thermal effect is mitigated through efficient thermal dissipation, fast nonlinearity such as FCE in silicon may dominate (*23*, *31*), opening doors to nonreciprocal high-speed optical signal processing where instantaneous response is required.

Our optical diode utilizes only the materials already used in CMOS processing, and does not require external assistance such as magnetic fields, radio-frequency modulation, or optical pumping. The broad input power range within which our device performs may be sufficient for on-chip photonic applications. Its ability to block backward input much stronger than the forward input makes it functionally similar to electrical diodes. Our diode has an ultra-compact footprint and is robust against resonance mismatch between the two microrings. These attributes make it attractive as a potential component for future highly-integrated photonic information processing chips.

References and Notes

1. H. A. Haus, *Waves and Fields in Optoelectronics* (Prentice-Hall, Englewood Cliffs, NJ, 1984), pp. 56–61.
2. R. L. Espinola, T. Izuhara, M. C. Tsai, R. M. Osgood Jr., H. Dötsch, *Opt. Lett.* **29**, 941 (2004).
3. T. R. Zaman, X. Guo, R. J. Ram, *Appl. Phys. Lett.* **90**, 023514 (2007).
4. L. Bi *et al*., *Nat. Photonics* **5**, 758 (2011).
5. S. F. Mingaleev, Y. S. Kivshar, *J. Opt. Soc. Am. B* **19**, 2241 (2002).
6. K. Gallo, G. Assanto, K. R. Parameswaran, M. M. Fejer, *Appl. Phys. Lett.* **79**, 314 (2001).
7. M. Soljačić, C. Luo, J. D. Joannopoulos, S. Fan, *Opt. Lett.* **28**, 637 (2003).
8. A. Rostami, *Opt. Laser Technol.* **39**, 1059 (2007).
9. S. K. Ibrahim, S. Bhandare, D. Sandel, H. Zhang, R. Noe, *Electron. Lett.* **40**, 1293 (2004).
10. J. Hwang *et al*., *Nat. Mater.* **4**, 383 (2005).
11. S. Manipatruni, J. T. Robinson, M. Lipson, *Phys. Rev. Lett.* **102**, 213903 (2009).
12. Z. Yu, S. Fan, *Nat. Photonics* **3**, 91 (2009).
13. M. S. Kang, A. Butsch, P. S. J. Russell, *Nat. Photonics* **5**, 549 (2011).
14. B. E. Little, S. T. Chu, H. A. Haus, J. Foresi, J.-P. Laine, *J. Lightwave Technol.* **15**, 998 (1997).
15. Q. Xu, B. Schmidt, S. Pradhan, M. Lipson, *Nature* **435**, 325 (2005).
16. S. Xiao, M. H. Khan, H. Shen, M. Qi, *Opt. Express* **15**, 14467 (2007).
17. S. Xiao, H. Shen, M. H. Khan, M. Qi, *Conf. Lasers and Electro-Optics* CTuGG6 (2008); www.opticsinfobase.org/abstract.cfm?uri=CLEO-2008-CTuGG6.
18. T. Barwicz *et al*., *Opt. Express* **12**, 1437 (2004).
19. M. H. Khan *et al*., *Nat. Photonics* **4**, 117 (2010).
20. M. Soljačić, M. Ibanescu, S. G. Johnson, Y. Fink, J. D. Joannopoulos, *Phys. Rev. E* **66**, 055601 (2002).
21. P. E. Barclay, K. Srinivasan, O. Painter, *Opt. Express* **13**, 801 (2005).
22. T. Uesugi, B.-S. Song, T. Asano, S. Noda, *Opt. Express* **14**, 377 (2006).
23. Q. Xu, M. Lipson, *Opt. Lett.* **31**, 341 (2006).
24. J. Ouyang, X. Wang, M. Qi, Meep (MIT Electromagnetic Equation Propagation), http://nanohub.org/resources/2954 (2007).
25. See supporting material on *Science* Online.
26. V. R. Almeida, M. Lipson, *Opt. Lett.* **29**, 2387 (2004).
27. P. Sun, R. M. Reano, *Opt. Lett.* **35**, 1124 (2010).
28. X. Chen, N. C. Panoiu, I. Hsieh, J. I. Dadap, R. M. Osgood, *IEEE Photon. Technol. Lett.* **18**, 2617 (2006).
29. J. B. Driscoll *et al*., *IEEE J. Sel. Top. Quantum Electron.* **16**, 1448 (2010).
30. M. Dinu, F. Quochi, H. Garcia, *Appl. Phys. Lett.* **82**, 2954 (2003).
31. A. C. Turner-Foster *et al*., *Opt. Express* **18**, 3582 (2010).

Acknowledgments: We thank Dr. Daniel E. Leaird for experimental assistance and Jing Ouyang for helpful

discussions. The work was supported by Defense Threat Reduction Agency grant HDTRA1-10-1-0106, Air Force Office of Scientific Research grant FA9550-08-1-0379, National Science Foundation grant ECCS-0925759, and National Institute of Health grant 1R01RR026273-01. FDTD simulation work was carried out through the Network for Computational Nanotechnology (NCN) with resources available at www.nanohub.org. L.F. and L.T.V. fabricated and characterized the devices. J.W. performed simulation and selected device parameters. H.S. helped in device characterization. B.N. helped in the design. M.Q. conceived the idea and supervised the investigation. M.Q., L.T.V., L.F and J.W. wrote the manuscript. All discussed the results and commented on the manuscript.

Supporting Online Material

www.sciencemag.org/cgi/content/full/science.1214383/DC1
Materials and Methods
Table S1

23 September 2011; accepted 6 December 2011
Published online 22 December 2011;
10.1126/science.1214383

Fig. 1. (**A**) The optical diode consists of two resonance-matched notch filter (NF) and add-drop filter (ADF). Input at Port I and output at Port II is designated as forward propagation while input at Port II and output at Port I is defined as backward propagation. (**B** and **C**) Fabricated NF and ADF showing the design parameters. A titanium heater allows tuning of the NF resonance to match that of the ADF. (**D** to **G**) Mechanism of passive optical non-reciprocity (ONR) due to nonlinearity. The optical power at Port I, Center Point and Port II are defined as $P_{in,f}$, $P_{c,f}$, and $P_{out,f}$ for the forward direction and as $P_{out,b}$, $P_{c,b}$, and $P_{in,b}$ for backward propagation. Dashed curves are the simulated transmission spectra in the linear regime (~85 nW incident power) while the solid curves are the simulated transmission spectra at a power level ~85 μW, which is high enough to induce optical nonlinearity. (**H**) Forward and backward transmission spectra of the diode at ~85 nW incident power, showing reciprocity and good agreement with dashed curves in (E) and (G). (**I**) Forward and backward transmission spectra at input power level ~85 μW, showing strong ONR and good agreement with solid curves in (E) and (G).

Fig. 2. Forward and backward transmission spectra of the all-Si optical diode at relatively high input power levels. (**A**) At ~850 μW input power (10 dBm at laser source). Solid curves were acquired through a continuous-mode scan, and dashed lines through a stepped-mode scan. The nonreciprocal transmission ratio (NTR) near 1630 nm is 27.3 dB for continuous-mode scan and 29 dB for step-mode scan. (**B**) At ~2,100 μW input power (14 dBm at laser source). The NTR near 1630 nm is 27 dB.

Fig. 3. Saturation of the backward transmitted power near resonance in an ADF with coupling gaps of 420 nm and 630 nm.

Fig. 4. (**A**) Wavelength tunability and tolerance of the mismatch between resonant wavelengths of the two filters. Dashed lines are forward transmissions and solid lines are backward transmissions. Input power was ~2,100 μW. Inset shows explicitly the NTR. (**B**) The NTR at various input power levels with a fixed operating wavelength of 1630.011nm.

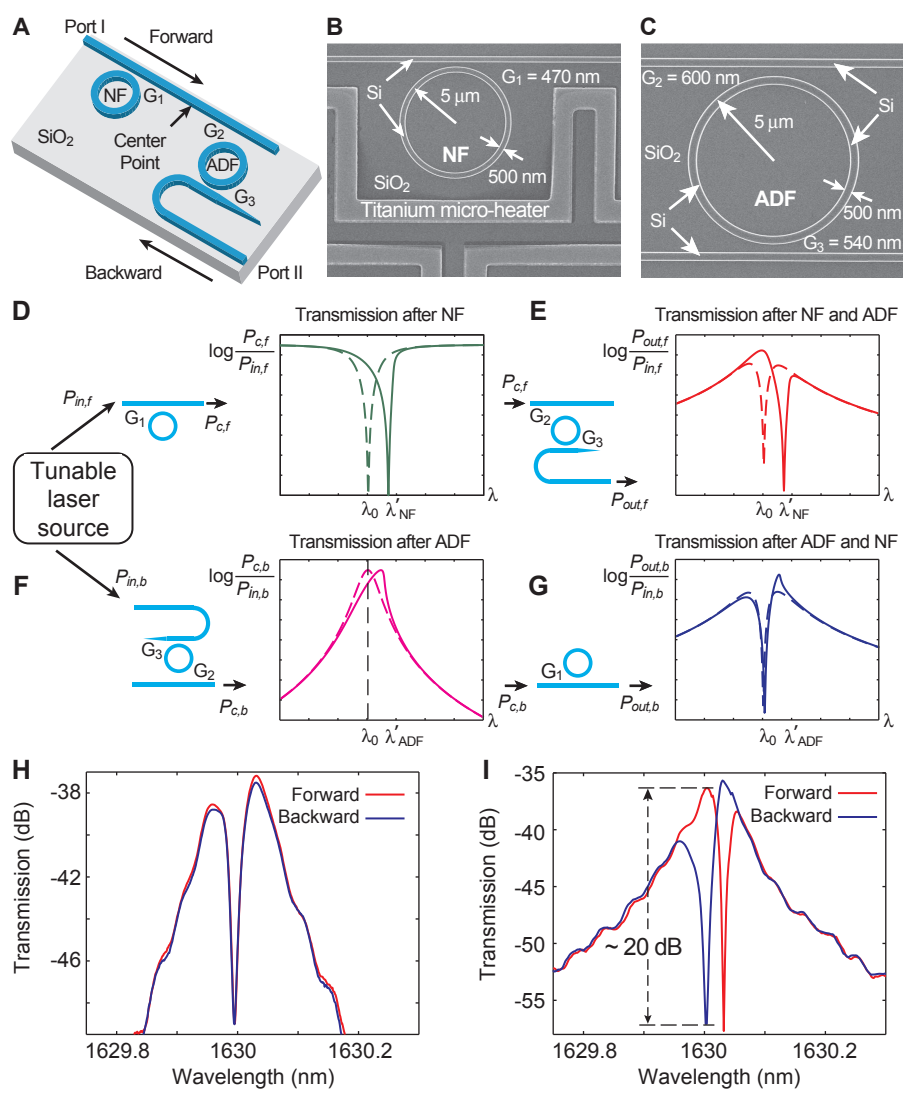
A
Port I
Forward
NF
G1
SiO2
Center
Point
G2
ADF
G3
Backward
Port II
B
Si
5 μm
G1 = 470 nm
NF
SiO2
500 nm
Titanium micro-heater
C
G2 = 600 nm
5 μm
Si
SiO2
ADF
Si
500 nm
G3 = 540 nm
D
Transmission after NF
log Pc,f / Pin,f
Pin,f
G1
Pc,f
Tunable laser source
λ0 λ'NF
λ
E
Transmission after NF and ADF
log Pout,f / Pin,f
Pc,f
G2
G3
Pout,f
λ0 λ'NF
λ
F
Transmission after ADF
log Pc,b / Pin,b
Pin,b
G3
G2
Pc,b
λ0 λ'ADF
λ
G
Transmission after ADF and NF
log Pout,b / Pin,b
Pc,b
G1
Pout,b
λ0 λ'ADF
λ
H
Transmission (dB)
-38
-42
-46
Forward
Backward
1629.8
1630
1630.2
Wavelength (nm)
I
Transmission (dB)
-35
-40
-45
-50
-55
~ 20 dB
Forward
Backward
1629.8
1630
1630.2
Wavelength (nm)

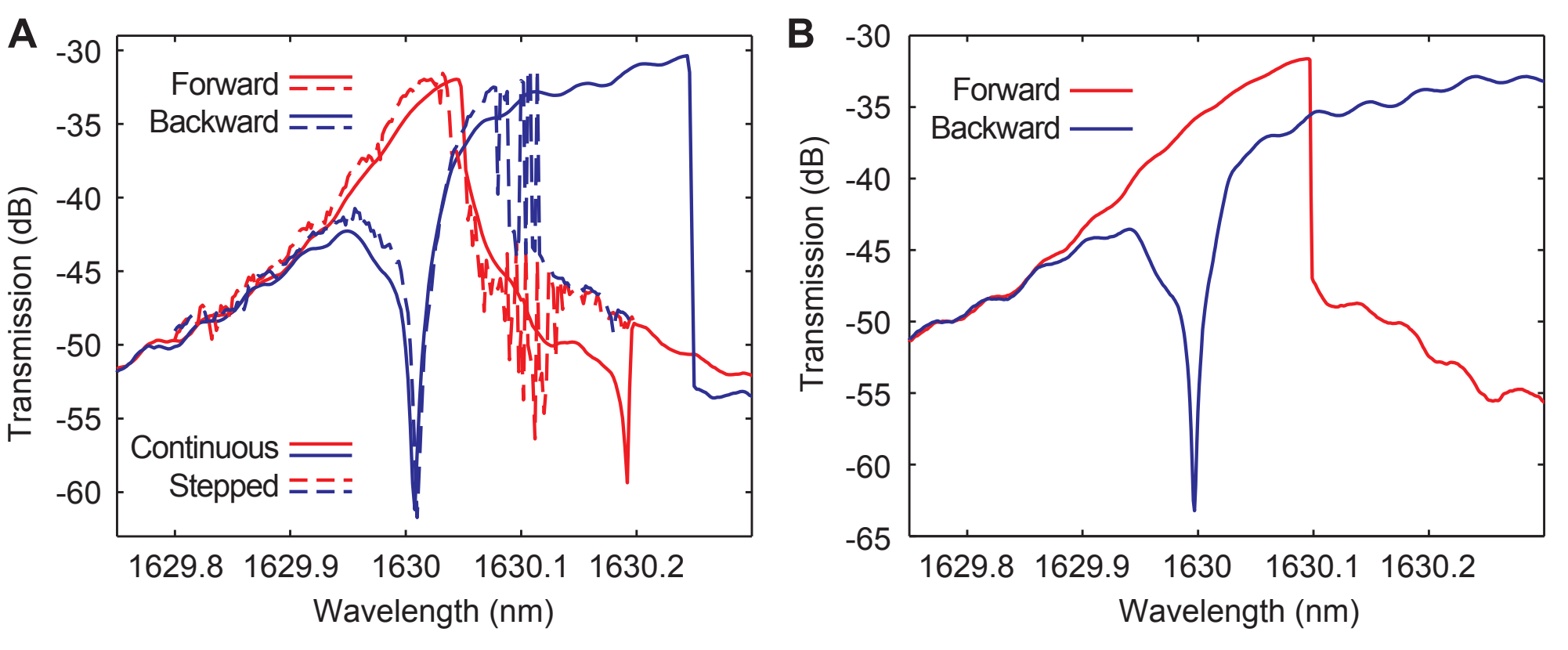
A
B
Forward
Backward
Continuous
Stepped
Transmission (dB)
Wavelength (nm)
-30
-35
-40
-45
-50
-55
-60
-65
1629.8
1629.9
1630
1630.1
1630.2

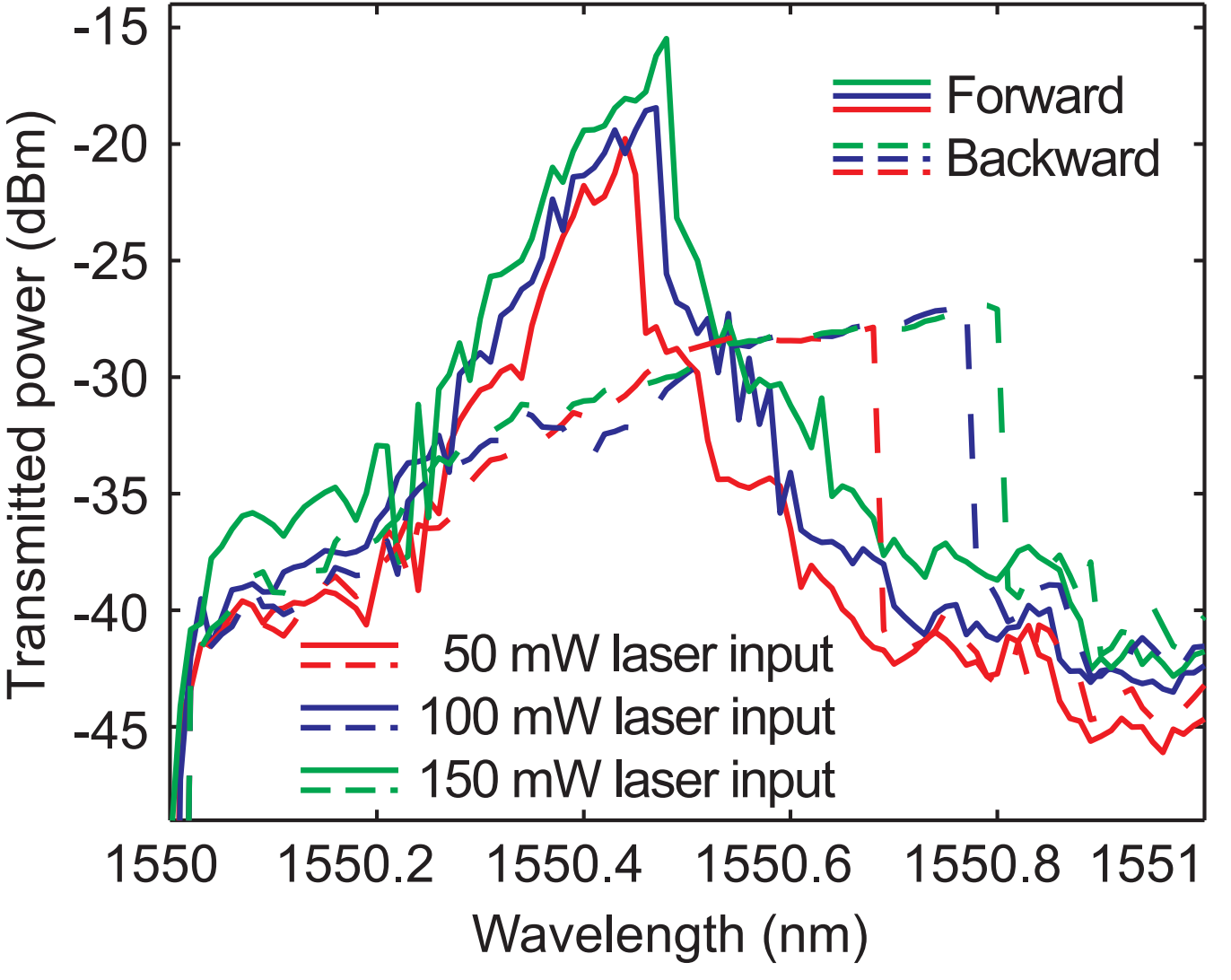
-15
-20
-25
-30
-35
-40
-45
Transmitted power (dBm)
Forward
Backward
50 mW laser input
100 mW laser input
150 mW laser input
1550
1550.2
1550.4
1550.6
1550.8
1551
Wavelength (nm)

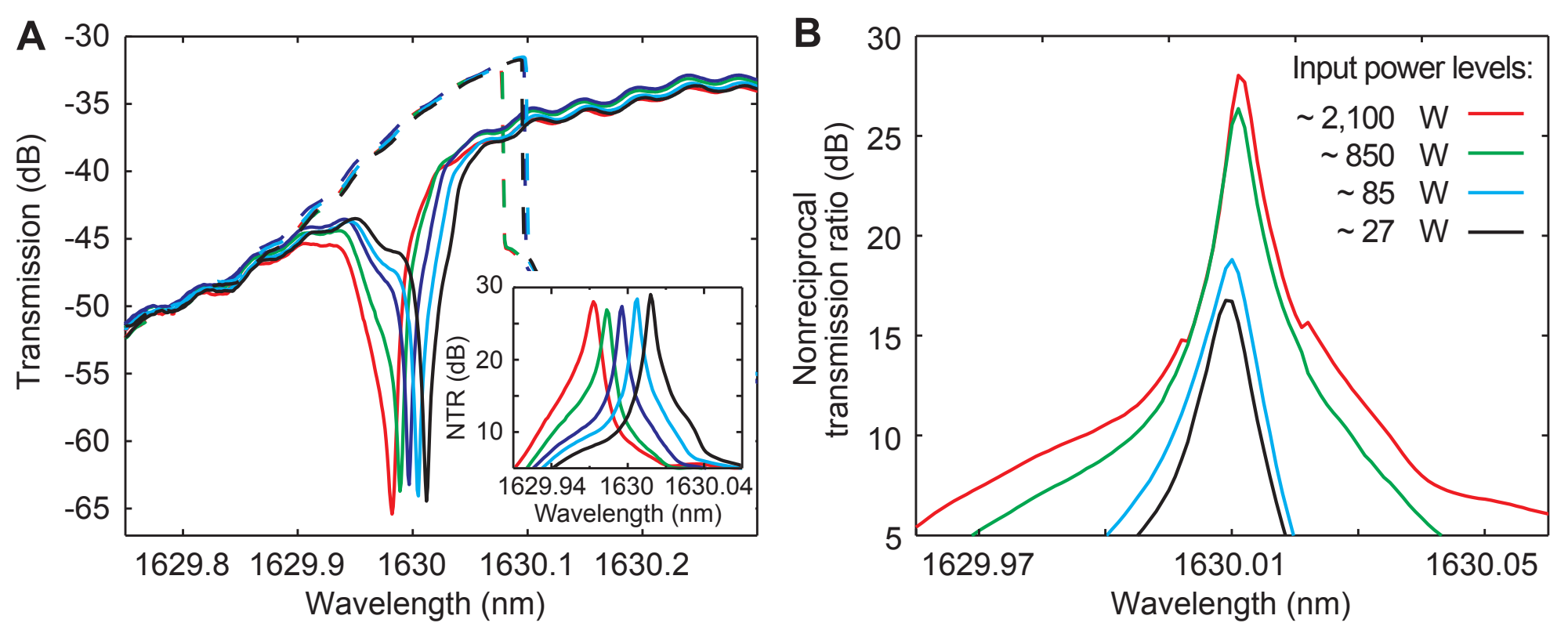
A
Transmission (dB)
-30
-35
-40
-45
-50
-55
-60
-65
1629.8
1629.9
1630
1630.1
1630.2
Wavelength (nm)
NTR (dB)
30
20
10
1629.94
1630
1630.04
Wavelength (nm)
B
Nonreciprocal transmission ratio (dB)
30
25
20
15
10
5
1629.97
1630.01
1630.05
Wavelength (nm)
Input power levels:
~ 2,100 W
~ 850 W
~ 85 W
~ 27 W